PCCP

Dynamic Article Links

Cite this: *Phys. Chem. Chem. Phys.*, 2011, **13**, 12603–12613

www.rsc.org/pccp

PAPER

Effective interaction between charged nanoparticles and DNA

Fabien Paillusson,[bc] Vincent Dahirel,[a] Marie Jardat,[a] Jean-Marc Victor[bc] and Maria Barbi*[bc]

Received 7th February 2011, Accepted 13th April 2011
DOI: 10.1039/c1cp20324j

We investigate the effective interaction mediated by salt ions between charged nanoparticles (NPs) and DNA. DNA is modeled as an infinite cylinder with a constant surface charge in an implicit solvent. Monte Carlo simulations are used to compute the free energy of the system described in the framework of the primitive model of electrolytes, which accounts for excluded volumes of salt ions. A mean-field Poisson–Boltzmann theory also allows us to compute the free energy and provides us with explicit formulae for its main characteristics (position and depth of the minimum). We intend here to identify the physical parameters that have a major impact on the NP–DNA interaction, in an attempt to evaluate physico-chemical properties which could play a role in genotoxicity or, which could be exploited for therapeutic use. Thus, we investigate the influence on the effective interaction of: the shape of the nanoparticle, the magnitude of the nanoparticle charge and its distribution, the value of the pH of the solution, the magnitude of Van der Waals interactions depending on the nature of the constitutive material of the NP (metal *vs.* dielectric). We show that for positively charged concave NPs the effective interaction is repulsive at short distance, so that it presents a minimum at distance from the DNA. This short-range repulsion is specific to indented particles and is a robust property that holds for a large range of materials and charge densities.

Introduction

A crucial point of the regulation of cell functions is the role of the diffusion of the network active agents (proteins, enzymes) and the effect of this diffusion on the network kinetics. One of the key quantities controlling the kinetics of reactions involving DNA is the time needed for a reactant to find its target sequence through the complex three-dimensional cell architecture. As is nowadays widely accepted, the search mechanism of DNA-binding proteins is accelerated by the combination of a 3-dimensional diffusion in the bulk and the so-called "sliding" process.[1–5] The sliding involves a non-specific binding of the protein to the DNA, far from the target site, followed by a 1D diffusion along the molecule until the enzyme possibly reaches the specific sequence, or else enters a new run of 3D diffusion, and sliding again and again until it eventually reaches the specific sequence. The probability of it encountering the specific sequence is enhanced by reducing the dimension of the explored space. Under this scenario, the protein interacts most of the time with non-specific DNA sequences (until it reaches the specific target sequence) and the predominance of electrostatics during the sliding process is unquestionable.[6–11] We recently showed[12] using Monte Carlo simulations and analytical calculations, that a counterintuitive repulsion exists between the DNA and an oppositely charged protein at nanometre range. For the concave shape of DNA binding proteins, and for realistic protein charge densities, the DNA–protein interaction free energy has a minimum at a finite surface-to-surface separation, in which proteins can easily slide. In this study we only considered proteins with fixed charges, at a unique salt concentration corresponding to the usual physiological conditions (salt concentration of 0.1 mol L^{-1}). Moreover, we did not investigate the role of Van der Waals interactions between the protein and DNA.

We intend here to extend our results of the DNA–protein interaction to any kind of nanoparticle (NP) interacting with DNA. Indeed, a number of recent papers deal with the insertion of inorganic NP in biological media, be it for the development of contrast agents in cellular imagery,[13,14] for their use in drug-delivery processes,[15] or to investigate their possible toxicity.[16,17] In these examples, the involved NP are usually charged, but with a surface charge density which can be pH-dependent. Furthermore, the characterization of DNA–NP interactions is often experimentally performed

[a] *UPMC Univ Paris 06, UMR CNRS 7195, PECSA, F-75005 Paris, France*
[b] *UPMC Univ Paris 06, UMR 7600, Laboratoire de Physique Théorique de la Matière Condensée, F-75005 Paris, France. E-mail: barbi@lptl.jussieu.fr*
[c] *CNRS, UMR 7600, F-75005 Paris, France*

under non-physiological conditions. Finally, physiological pH and salt concentration can vary extensively around their averaged values, and these averaged values may depend on the organism or on the cell type. In this context, we propose in the present paper to characterize extensively the influence of the salt concentration and of the pH on the interaction. Moreover, we proceed during our investigation into the influence of shape and of surface charge density of the NP on DNA–NP interaction, detailing some aspects overlooked in a previous study, such as the effect of charge distribution.

We treat the system in the framework of the primitive model (also refered to in the literature as the continuous solvent model or as the implicit solvent model), where the solvent is implicitly described by its dielectric constant. The electrodynamic Van der Waals contribution reflects quantum and thermal charge fluctuations effects on the interaction. We have chosen to compute this term using an analytical theory. The electrostatic interaction between a nanoparticle and a DNA molecule includes an averaged contribution from the micro-ions surrounding the nanoparticle and the DNA (*i.e.* the salt ions and the counter-ions). This term is not straightforward to compute, as it depends on the equilibrium distribution of a large number of particles interacting through long range forces. In order to compute the effective interaction between model DNA and nanoparticles averaged over the micro-ions configurations, two computational techniques are used here which differ mostly in the treatment of the micro-ions present in the solution. We first run Monte Carlo simulations, where the excluded volume of the micro-ions and all N-body correlations between micro-ions are taken into account. We also perform analytical calculations, using the Poisson–Boltzmann theory. This theory is a mean field approximation and treats micro-ions as point-like charges. Our strategy is the following: we fit the value of some parameters of the analytical Poisson–Boltzmann calculations to obtain the best agreement with Monte Carlo calculations. Thus, we obtain an explicit analytical formula of the effective interaction between DNA and the charged nanoparticle, which gives the position of the minimum and its depth. We can then investigate the influence of some physical parameters on the interaction free energy, like the salinity of the medium or the pH of the solution. We also quantify the range and magnitude of Van der Waals interactions compared to Coulombic ones. Finally, we obtain a complete picture of the effective interaction between charged nanoparticles and DNA, and of the main parameters which control the range and the intensity of the interaction free energy. These results may be useful in the context of the drug design.

The paper is organized as follows. Section I is devoted to the modeling of the system and to technical details concerning our Monte Carlo simulations and our analytical calculations. Section II presents the results of the Monte Carlo simulations. Section III is devoted to the comparison between the analytical calculations and the simulations. Section IV investigates the influence of the pH on the effective interaction. In Section V the range and the magnitude of Van der Waals interactions compared to Coulombic ones is discussed and our conclusions are presented.

I. Methods and coarse-grained models of the system

A. Coarse grained model

Several recent studies of the protein–DNA interaction during target search relies on spring-beads models for the macromolecules—sometimes at the scale of the residues—whereas the electrostatic interaction just reads as a sum of Debye–Hückel pair potentials between the spherical beads,[18–20] namely DLVO electrostatic pair potentials.[21] These potentials of mean force work well in standard colloid physics when dealing with spherical particles of the same charge and when the mean inter-particle distance is much bigger than the Debye length. But, such approximated interactions are not supposed to be valid when the weak overlap approximation[22–24] fails *i.e.* when the counter-ion cloud around the protein interacts with DNA charges. Here, we propose to resort to a coarse-grained model of the system which mainly focuses on the electrostatic properties of all the particles of the system, including the micro-ions of the physiological medium, but not on the internal degrees of freedom of the DNA. The advantage of this model is that it takes into account micro-ion correlations as well as osmotic pressure effects on the charged bodies contrary to the above cited works. The persistence length of DNA (*i.e.* the basic mechanical property quantifying the stiffness of a long polymer[25]) is about 50 nm under physiological conditions. Since the length scale is given by the typical size of a DNA-binding protein or a NP, *i.e.* a few nanometres, the DNA molecule is approximately straight at this scale. Moreover, DNA is highly negatively charged: double stranded DNA has a net charge of $-2e$ per base pair. This leads to a linear charge of $-e$ every 0.17 nm or, equivalently, to an average surface charge density $\sigma_{\mathrm{DNA}} = -1.0\, e\ \mathrm{nm}^{-2}$. We thus model DNA as a hard cylinder of radius 1 nm, with charges along the axis of the cylinder, on divalent sites separated by a distance of 0.34 nm, corresponding to the base pair step. From this, the angular anisotropy related to the major/minor grooves is therefore ignored.

We consider the effective interaction of this model DNA with charged nanoparticles (NPs). From our previous analysis on DNA-binding proteins,[12] based on the data set of 56 non-homologous proteins of ref. 7 and 26, we know that the main characteristic features of DNA-binding proteins leading to a non trivial interaction behavior with DNA is their positive charge (distributed over the interval $[0.1,0.4] \times |\sigma_{\mathrm{DNA}}|$) and their shape complementary with DNA, which leads to a large surface area of interaction ($15 \pm 5\ \mathrm{nm}^2$ on average). Inspired by these results, we model NPs as rigid bodies, positively charged, with a surface charge density in the range 0.1–0.4 $e\ \mathrm{nm}^{-2}$, and here, we address the issue of the particular role of the shape in the interaction of a designed NP with DNA.

We vary the charge and the shape of the NP, which is either a sphere or a hard core body with a cylindrical cavity. The curvature of this hard core cylindrical cavity (one nanometre wide, corresponding to the DNA diameter) is varied systematically (Fig. 1). In most cases investigated here, the charge of the NP is placed on a single site at a given distance

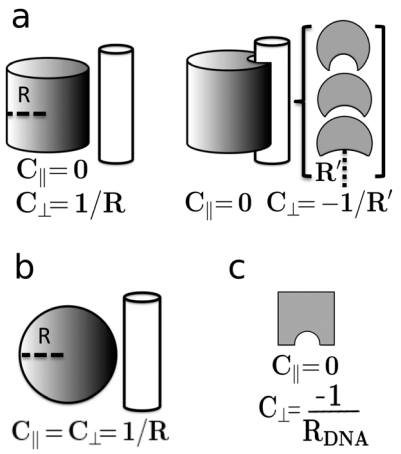

Fig. 1 Schematic view of the model nanoparticles. (a) Convex (left) and concave (right) cylindrical NPs; (b) spherical NP; (c) cubic NP. The height and diameter of the cylindrical NPs are both 5 nm, as well as the side of the cubic NP and the diameter of the spherical one. The hollow cylindrical NPs have a cylindrical cavity, of curvature $C_{\perp} = 0$, -0.25, -0.5 or -1 nm^{-1}. The hollow cubic NP has a cylindrical cavity of radius 1 nm, *i.e.* equal to the DNA radius.

under its surface facing DNA. The direct electrostatic force in vacuum is therefore the same for all the NP shapes investigated, this allows us to investigate the effect of the geometry on the ion-mediated interaction between the two bodies. Since the charge discretization and localization may play a role in the effective interaction, we have also designed different charge patterns at the NP surface and studied their effect.

Micro-ions of the physiological medium are modelled in the framework of the primitive model of electrolytes: micro-ions are charged hard spheres in an implicit solvent of relative electric permitivity $\varepsilon = 78.25$ (water). The primitive model of electrolytes explains the less intuitive trends of electrostatic interactions in solution, *e.g.* the attraction between like-charged particles,[27–29] or the repulsion between charged and neutral ones.[30] Except when it is specified, the salt concentration of the solutions corresponds to physiological conditions ($\sim$0.1 mol L^{-1}). The influence of the micro-ion concentration is considered in Section IV. Micro-ions are here monovalent ions with a radius of 1.5 Å which is the typical size of sodium and chloride ions in the primitive model of electrolyte solutions.

The dielectric constants of the DNA and the NP are fixed to the solvent, according to the so called "homogeneous dielectric constant model (HDM)" so as to avoid dielectric discontinuities. This has been shown to have little incidence on the effective interaction between small hydrophilic proteins.[31] Nevertheless dielectric discontinuities could be taken into account in an improved version of the model both for PB calculation and Monte Carlo simulation.[32,33]

B. Monte Carlo simulations

To compute the effective interaction between DNA and NP, we use Monte Carlo simulations. The model DNA, NP and micro-ions are placed in a parallel epipedical simulation box ($27.5 \times 27.5 \times 15$ nm) with periodic boundary conditions. The potential of mean force between the two bodies, DNA and NP, separated by a distance L is equal to the free energy of the global system (NP, DNA and ions in water). At a fixed surface-to-surface distance L, this free energy only depends on the ion distribution and is therefore computed using MC simulations sampling the ion configurations.[34,35] MC simulations are carried out in the NVT ensemble, with $T = 298$ K. Additional results from μVT simulations are obtained for ten randomly chosen cases and they are undistinguishable from NVT results. We voluntarily froze the rotational degrees of freedom of the NP, and studied the interaction for the most attractive orientation, *i.e.* when the NP cavity points toward DNA. This assumption overlooks the rotational entropic cost when the NP gets closer to DNA and hence underestimates the repulsion. However, we could estimate numerically (data not shown) that the semi-quantitative picture resulting from this study still holds when the rotational degrees of freedom of the NP are accounted for. Given the cylindrical symmetry of the model DNA we choose L as the reaction coordinate, the surface-to-surface distance for the most attractive orientation (the surfaces being the ion-accessible surfaces). The methodology used to compute the ion-averaged forces is described in detail[28,34]. Each value of force is averaged over 8×10^8 to 10^9 MC steps. We took particular care to assess the statistical errors from our simulations. The forces are thus computed: (i) on the NP and on the DNA (to check Newton's Third law), (ii) with a twofold simulated time and (iii) from independent initial configurations.

The free energy profiles obtained from these MC simulations are presented in Section II.

C. Poisson–Boltzmann approach

In the previous section we have shown that MC simulations allow the free energy of the NP–DNA system to be obtained, and describe the main features of their interaction. MC simulations are however rather time-consuming. In order to make a more systematic study of the NP–DNA system, including the effect of varying pH (see Section IV) and salt conditions, we introduce an analytical approach, based on the Poisson–Boltzmann theory. Moreover, this approach allows us to obtain analytical formulae for the free energy minimum depth and position, and to give more insight into the physics of the repulsion.

1. Derjaguin approximation. The simplest theoretical counterpart of the above mentioned MC simulations program is to solve the non linear PB equation for each NP shape and then deduce the free energy landscape in each case. This is mean field theory and solving this problem often requires intensive numerical calculations.[36] To further simplify the problem it is common to rely on a proximity force approximation, namely the Derjaguin approximation,[21] to estimate the interaction between two charged NPs at short distance. In this approximation once denoted by L, the distance of closest approach between two curved surfaces, the corresponding free energy $E(L)$ between the two surfaces is evaluated approximately starting from the interaction free energy per unit area $W(h)$ between two flat plates at a distance h as

$$E(L) \approx \int_A W(h)\mathrm{d}A \qquad (1)$$

where the integral is over the area A of the surfaces facing each other, and the distance h is a function of the position of the differential surface element δA over the surface. In the following, we use the Derjaguin approximation for two cases of a spherical NP and a perfectly matching concave NP (Fig. 1). The integration is done over the NP area following the procedure explained in textbooks.[21]. The case of complementary shapes is the simplest one. In this case, the free energy $E(L)$ is proportional to $W(L)$, because the distance between two surface elements of the macromolecules facing each other is constant and equal to L. More explicitly, if S_{int} is the surface of interaction of the concave body, the free energy is simply given by

$$E(L) \approx S_{\text{int}} W(L) \tag{2}$$

For the case of a spherical NP, the integration can be performed numerically, once having explicitly written the surface-to-surface h for any position on the surfaces.

2. PB resolution of the planar problem. We therefore consider a model in which both the NP and the DNA are, at first, represented by uniformly charged, parallel, infinite and planar surfaces facing each other. We introduce the position variable x such that the two plates are at $x = 0$ and $x = L$, respectively, and indicate the surface charge densities as σ_{DNA} and σ_{NP}. The resulting problem is analytically solvable; the actual geometry of the two interacting surfaces are taken into account using the Derjaguin procedure.

We compute the free energy per unit area $W(L)$ under a mean field approximation, assuming that sufficiently diluted solutes and moderate electric fields, reduce to the Poisson–Boltzmann (PB) theory.[37] Using this framework, the pressure at position x between the plates takes the simple form:[38,39]

$$P(x) = -\frac{\varepsilon}{2}\left(\frac{\mathrm{d}\phi(x)}{\mathrm{d}x}\right)^2 + k_{\text{B}}T\sum_{\alpha} n_{\alpha}(x) \tag{3}$$

where k_{B} is the Boltzmann constant, T the temperature, $\phi(x)$ the electrostatic potential field and $n_{\alpha}(x)$ is the average density of ions of type α at position x. Note that the first term is the classical electrostatic pressure and the second corresponds to the osmotic pressure due to ions in solution, when they are assumed to behave like an ideal gas as is the case in any mean field approximation for a dilute system. Then, assuming that the ionic densities follow Boltzmann distributions, we obtain the well-known Poisson–Boltzmann equation:

$$\beta e\frac{\mathrm{d}^2\phi(x)}{\mathrm{d}x^2} = 4\pi\ell_{\text{B}}\{2n_b \sinh(\beta e\phi(x))\}, \tag{4}$$

to be solved with the boundary conditions

$$\lim_{x\to 0}\beta e\frac{\mathrm{d}\phi}{\mathrm{d}x} = -4\pi\ell_{\text{B}}\sigma_{\text{DNA}}, \tag{5}$$

$$\lim_{x\to L}\beta e\frac{\mathrm{d}\phi}{\mathrm{d}x} = 4\pi\ell_{\text{B}}\sigma_{\text{NP}}. \tag{6}$$

In previous equations $\ell_{\text{B}} \equiv e^2/4\pi\varepsilon k_{\text{B}}T$ is the Bjerrum length, and $n_{\text{b}} = n_{\text{b}-} = n_{\text{b}+}$ is the bulk concentration for a 1 : 1 electrolyte.

It is worth noting that solutions containing polyvalent ions require the introduction of fluctuations and correlations, which are neglected in the mean field approximation by definition, this limits the validity of the Boltzmann distribution in this case. Various system dependent coupling parameters can be found to rationalize the range of validity of the PB theory.[40,41] However, PB theory is known to lead to reliable results for monovalent solutions, as those considered in our work.

The explicit computation of the solution of the non-linear ODE eqn (4) is impossible because it involves elliptic integrals[36] together with implicit equations that need to be numerically solved. Therefore, we directly solve eqn (4) with eqn (6) numerically using the Maple solver. Once $\phi(x)$ is obtained, the calculation of the pressure between the two plates follows from eqn (3). As in all systems at equillibrium, the total pressure P is homogeneous, *i.e.* $P(x)$ is the same at any $x \in [0;L]$, for given L, so that we can write it $P(L)$. By numerical integration of the excess pressure between the plates, $P(L) - 2n_{\text{b}}k_{\text{B}}T$, we then get $W(L)$, the free energy per unit area between the plates.

II. Results obtained by Monte Carlo simulations

1. The shape of the nanoparticle highly influences the free energy profile. As mentioned in the previous section, we first studied the influence of NP shape on the interaction free energy, for a constant NP charge. Starting with a cylindrical shape of both diameter and height of 5 nm, we modified the NP curvature in the perpendicular direction ($C_{\perp}$) by creating a cylindrical cavity on one side of the solid (Fig. 1). In every case, the charge of the NPs is given by a single $+5e$ site placed 0.7 nm under the NP surface facing DNA. The free energy computed from Monte Carlo (MC) simulations as a function of the surface-to-surface distance L is reported in Fig. 2. The effect of the transverse curvature $C_{\perp}$ is remarkably pronounced: the free energy as a function of L, which is monotonic for $C_{\perp} > 0$, becomes non-monotonic for $C_{\perp} < 0$ and exhibits then a minimum E_{min} at a distance L_{min}. For $L < L_{\text{min}}$, there is an unexpected repulsive free

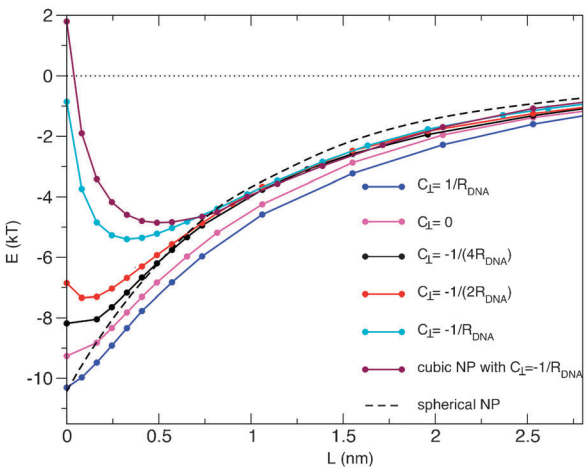

Fig. 2 Influence of shape of the nanoparticle on the interaction. Free energy of the DNA–NP systems computed by MC simulations. The NPs and DNA are immersed in a monovalent salt whose Debye length $\lambda_D = 1$ nm corresponds to physiological conditions (0.1 mol L^{-1}). Except when specified, the NPs are cylindrical, as depicted in Fig. 1a. The standard deviation of the free energy is 0.2 $k_{\text{B}}T$.

energy barrier between the oppositely charged bodies, that reaches $\sim 5k_BT$ in the case of perfectly matching surfaces ($C_\perp = -1/R_{DNA}$). This behavior is robust: the free energy curve is only weakly influenced by the shape of the remaining surface of the NP, as can be seen by comparing with the case of a cubic hollow NP, for which E_{min} varies by approximately 0.5 k_BT with respect to the corresponding cylindrical case. The effect of a variation in the curvature along the DNA direction (noted $C_\parallel$) is also investigated. Again, $C_\parallel$ only slightly influences the range of the interaction, as illustrated by the comparison of spherical and cylindrical convex NPs (Fig. 2). Therefore, we show here that the short range interaction between two oppositely charges bodies in solution strongly depends on their shape in the following way: it is attractive in the case of two convex bodies, but it becomes repulsive for complementary shapes, the strongest effect being observed for perfect matching shapes.

2. The charge of the NP influences the interaction but its distribution does not. We now focus on the perfectly matching concave NP ($C_\perp = -1/R_{DNA}$), where the strongest repulsion is observed, and allow the NP surface charge density σ_{NP} to vary. This parameter strongly modulates the free energy profile, as shown in Fig. 3. For an interface of *e.g.* 15 nm^2, if σ_{NP} changes from $0.13|\sigma_{DNA}|$ to $0.39|\sigma_{DNA}|$, E_{min} dramatically decreases from -2 k_BT to -14 k_BT and L_{min} decreases from 0.75 nm to 0.1 nm. Not surprisingly, the effect of the increasing NP charge is to widen and deepen the free energy minimum, *i.e.* to increase the attraction. In a less straightforward way, the equilibrium position moves closer to the DNA surface.

To have more insight into the possible effects induced by the model, we performed systematic modifications of the charge pattern on the NP. The effect of the charge discretization and distribution is studied by changing the number of charged sites N while keeping the NP charge Z_{NP} constant (see Fig. 4 for results and the different charge patterns). The free energy is found to be an independent function of N and of the geometry of the charge pattern within statistical errors. These results also show that the free energy does not depend on the coordinate along DNA. Furthermore, the addition of charged sites at the surface of the NP but far from the interface induces minor changes (blue curve). In conclusion, when the pattern changes at constant interface charge density σ_{NP}, the free energy exhibits only minor variations.

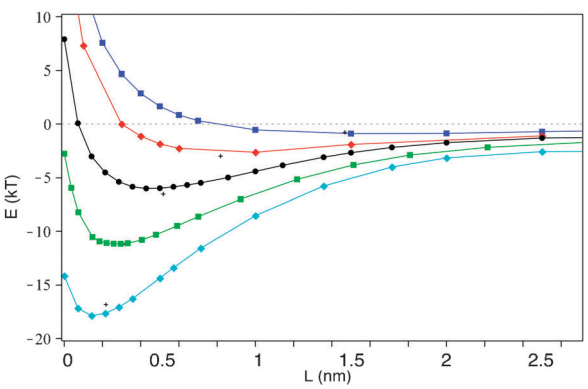

Fig. 3 Influence of the charge of the nanoparticle on the interaction. Free energy of the DNA–NP system for a set of NP charge densities, as obtained by MC simulations. From top to bottom: $\sigma_{NP}/|\sigma_{DNA}| = 0.06, 0.13, 0.19, 0.26, 0.32$. The area of the interface is 15 nm^2. The shape model for the NP is a cylinder of height 5 nm, with a concave interface ($C_\perp = -1/R_{DNA}$, $C_\parallel = 0$). The charges are distributed on a pattern of 16 sites, 0.1 nm below the surface.

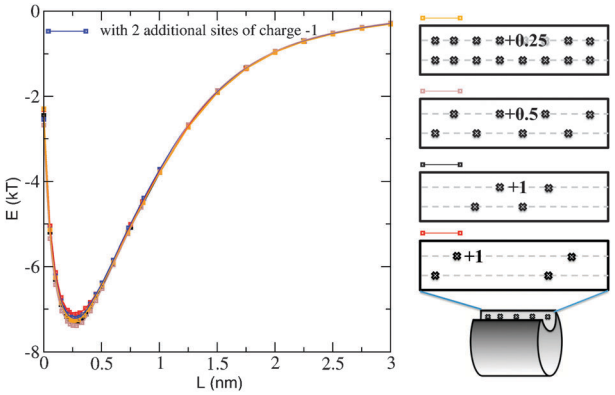

Fig. 4 Influence of the charge distribution of the nanoparticle on the interaction. The free energy is obtained for different charge patterns corresponding to the same charge density: $N = 16$ (orange curve), $N = 8$ (brown), and $N = 4$ with two different geometries of the charge pattern (black, red). The blue curve corresponds to the addition of two charged sites at the surface of the NP but far from the interface.

III. Comparison with the PB theory

1. Effective parameters can be fitted to account for MC results. We now compare the previous results to those obtained by direct integration of the PB equation together with the use of the Derjaguin approximation. Since this disregards completely the surface geometry and the precise position of charges, the planar approximation is expected to induce systematic errors in the ion concentration near the convex and concave surfaces. Such effects are, however, accounted for by a suitable charge renormalization. We rescale the DNA and NP charge densities for the two cases of the spherical and of the perfect matching concave NP. The fitting parameter is fixed so as to fit the value of the surface-to-surface distance and free energy value at the minimum obtained by MC simulations. For all considered cases we use the same rescaled DNA charge density of $\sigma_{DNA}^{eff} \simeq 0.6\sigma_{DNA}$. The NP charge density is rescaled instead by using two different effective parameters for the case of a spherical NP and for the case of a shape that matches perfectly the DNA cylinder. A comparison with the corresponding MC results in Fig. 2 are reported in Fig. 5, these show that the simple PB theoretical model reproduces the observed behavior for NP of different shapes rather well, provided that effective parameters are used for their charge density. Moreover, the *same* rescaling factors for both the DNA and the convex NP charge densities allows us to fit each of the free energy profiles, presented in Fig. 3, where the NP charge density is varied while the shape is kept unchanged.[12] This proves that charge density rescaling is a genuine geometry-dependent feature.

It can be noticed, finally, that the effective charge density for the sphere (0.4 e nm^{-2}) is higher than for the concave

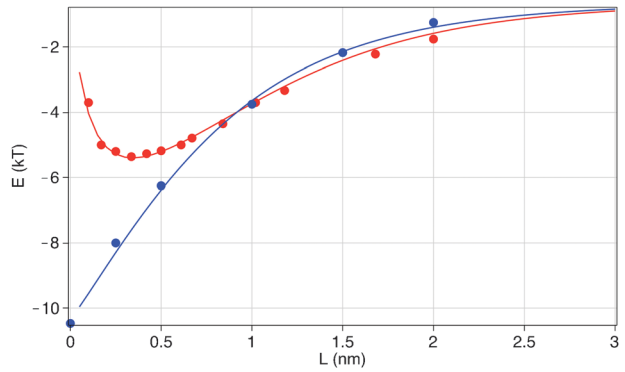

Fig. 5 Comparison between MC curves (Fig. 2) and PB theory curves within the Derjaguin approximation. Plot of the free energy *vs.* the surface-to-surface distance. Blue and red points correspond to MC simulation results, respectively, for a sphere and for a DNA-matching shape. Blue and red lines correspond to the Derjaguin approximation used on PB, results for two plates standing for the spherical NP and the DNA-matching one, respectively. The curves' fit were obtained with the parameters: $\sigma^{\text{eff}}_{\text{sphere}} = 0.4\ e\ \text{nm}^{-2}$ for the spherical NP and $\sigma^{\text{eff}}_{\text{conc}} = 0.18\ e\ \text{nm}^{-2}$ for the DNA-matching one.

cylinder-matching shape ($0.18\ e\ \text{nm}^{-2}$). This can be related to their respective interaction areas: indeed the interface area with the DNA cylinder is expected to be greater for a matching NP than for a sphere, thus leading to a smaller charge density.

2. Salt concentration influences the position and the depth of the interaction well for matching bodies. One advantage of the plate–plate PB theoretical approach is that parameters such as charge densities and salt concentration can be changed very easily. Moreover, the planar problem allows explicit analytical expressions to be calculated for the well depth and the position obtained in the framework of PB theory.[38] We recall that in the case of perfectly matching bodies, for which a short range repulsion is observed, the free energy is simply proportional to the free energy per unit area between the plates (eqn (2)). As a consequence, we can use these explicit expressions to directly estimate what the effect of the salt density is on the short range repulsive behavior. Let us introduce the range of the electrostatic interaction screened by the free charges in solution, *i.e.* the Debye length λ_D defined by $\lambda_D^{-2} = 4\pi\ell_B\sum_{i=1}^{2}\rho_i Z_i^2$, with ρ_i the concentration of ion i and Z_i the corresponding valence. We now define the two adimensional charge densities $\sigma'_{\text{DNA}} = 4\pi\ell_B\lambda_D\sigma^{\text{eff}}_{\text{DNA}}$ and $\sigma'_{\text{NP}} = 4\pi\ell_B\lambda_D\sigma^{\text{eff}}_{\text{NP}}$ and finally the adimensional charge parameter related to the *smallest* plate charge density, $\sigma'' = \min(\sigma'_{\text{DNA}},\sigma'_{\text{NP}})$. With these definitions, one gets:[38]

$$L_{\text{min}} = \lambda_D\left|\ln\left(\frac{|\sigma'_{\text{DNA}}|(2+\sqrt{\sigma'^2_{\text{col}}+4})}{|\sigma'_{\text{NP}}|(2+\sqrt{\sigma'^2_{\text{DNA}}+4})}\right)\right| \qquad (7)$$

$$E_{\text{min}} = \frac{4n_b\lambda_D S_{\text{int}}}{\beta}\left[\sqrt{|\sigma''|^2+4} - 2 - |\sigma''|\text{arcsinh}\left|\frac{\sigma''}{2}\right|\right] \qquad (8)$$

It is noteworthy that the well depth depends on the charge density of only one of the macromolecules whatever the salt concentration. As a consequence, if the NP charge density is lower than the DNAs, eqn (8) provides a simple way to obtain the NP rescaled charge density (in the case of matching bodies): it is enough to impose the equivalence between the right hand side of eqn (8) and the miminum value of the free energy obtained by MC simulations and solve for σ''.

The effect of salt concentration on the short range repulsion can be studied starting from eqn (7) and (8), and particularly by discussing the position of the free energy minimum. Contrary to E_{min}, L_{min} is a function of both charge densities. At the limit of zero salt concentration, it becomes independent of the ionic strength. Introducing the Gouy–Chapman lengths for both plates, $\lambda_{\text{NP}} = |1/2\pi\ell_B\sigma_{\text{NP}}|$ and $\lambda_{\text{DNA}} = |1/2\pi\ell_B\sigma_{\text{DNA}}|$. At low salt, $\lambda_D \gg \lambda_{\text{DNA}}$ and $\lambda_D \gg \lambda_{\text{NP}}$ and the well position for fixed charges is given by:

$$L_{\text{min}} \simeq |\lambda_{\text{NP}} - \lambda_{\text{DNA}}|\ \text{(low salt)} \qquad (9)$$

whereas for high salt concentrations it is:

$$L_{\text{min}} \simeq \lambda_D\left|\ln\left|\frac{\lambda_{\text{DNA}}}{\lambda_{\text{NP}}}\right|\right|\ \text{(high salt)}. \qquad (10)$$

The low salt regime distance in eqn (9) has a clear physical meaning since it corresponds to the situation where the counter-ion layers of each plate totally overlap. Also notice in eqn (10) that under high salt conditions the derivative of L_{min} with respect to λ_D is always positive, which suggests that the more salt added to the system the closer the short range repulsion is. These formulae are actually very useful to explain the physical origin of the repulsion, which is the purpose of the next subsection.

3. The presence of the well is due to competition between osmotic and electrostatic effects. The previous subsection sheds light on the two physical mechanisms responsible for the attraction and the repulsion. On one hand, when the distance between DNA and the NP decreases from infinity, their counter-ion clouds overlap, hence partially neutralize each other. The resulting salt excess is released into the solution with entropic gain. This effect reinforces the direct attraction between oppositely charged objects. This *salt release* regime has already been discussed elsewhere.[42] For a case when $\sigma_{NP} < |\sigma_{\text{DNA}}|$, the salt release continues until the anionic cloud is completely neutralized. When the distance between DNA and the NP is further decreased, a constant number of neutralizing cations remain confined between the charged bodies to maintain electroneutrality. Indeed, since the range of charge inhomogeneities in solution is λ_D, electroneutrality must be fulfilled at larger scales. As L decreases, these cations get more and more concentrated. Depending on the interaction area, the resulting enhancement of the osmotic pressure can exceed the electrostatic attraction and result in a global repulsion. The PB physical picture therefore explains the influence of complementary shape when compared to sphere–cylinder geometry: in the case of complementary shape the interface is large enough and the gap thin enough (relative to λ_D) to give rise to a net repulsion.[12]

IV. Influence of the pH in the case of matching bodies

1. Building a pH-dependent model. The net charge of a NP depends on the charging process. In particular, the solution pH can induce NP charge variation for cases where charges are carried by chemical groups with acidic or basic functions. In proteins for example, the charge is mainly due to the protonation/deprotonation of carboxylic and amino functions of the amino acids. In this case, the net charge is positive at low pH, zero at pH = pI and negative at high pH. For inorganic NP, the value of the pI depends on the nature of the chemical groups that give the charge. For iron oxide particles, pI $\simeq$ 7, with a positive charge at low pH and a negative one at high pH, but for silica particles, the pI is very low so that only negative charges are observed. Note that, in contrast, DNA is a strong acid, and therefore it maintains a constant charge practically at all relevant pH. In order to study the effect of pH on the NP–DNA interaction, the concentration of H^+ ions must be integrated in the model by an appropriate description. A complete picture of charge regulation effects goes far beyond the framework of this paper. The issue addressed here is whether the short range repulsion evidenced previously is robust with respect to charge regulation. For the sake of simplicity, we therefore focus on the specific example of a NP coated by neutral basic groups and we model the charging process as the adsorption of H^+ ions on the basic groups. The tendency to adsorb a proton for each one of these groups at a given pH is characterized by their pK. In the context of the one dimensional PB theory used throughout this work, this leads to a modified boundary condition on the plate corresponding to the NP. Indeed, the charge is now allowed to vary with respect to the distance L using the Langmuir adsorption term:[43]

$$\sigma_{\mathrm{NP}}(\mathrm{pH},\phi(L)) = \frac{\sigma^0_{\mathrm{NP}}}{1+10^{\mathrm{pH}-\mathrm{pK}}e^{\beta e\phi(L)}} \qquad (11)$$

with σ^0_{NP} the maximal possible surface charge of the NP. Note that $\sigma_{\mathrm{NP}} \simeq \sigma^0_{\mathrm{NP}}$ for pH < pK and $\sigma_{\mathrm{NP}} \simeq 0$ for pH > pK. At odds with this picture, the DNA charge density σ_{DNA} remains constant and negative. Taking the NP varying charge into account leads to the modified boundary conditions for the PB equation (eqn (4)):

$$\lim_{x\to 0} \beta e\frac{\mathrm{d}\phi}{\mathrm{d}x} = -4\pi\ell_{\mathrm{B}}\sigma_{\mathrm{DNA}}, \qquad (12)$$

$$\lim_{x\to L} \beta e\frac{\mathrm{d}\phi}{\mathrm{d}x} = 4\pi\ell_{\mathrm{B}}\sigma_{\mathrm{NP}}(\mathrm{pH},\phi(L)). \qquad (13)$$

2. Dependence of the interaction on pH–pK. We note from eqn (11) that, at a given ionic strength, the effect of pH on the effective NP charge only depends on the difference pH–pK. We therefore compute the plate–plate free energy as a function of pH–pK and inter-plate distance L by integrating eqn (4) with the boundary conditions eqn (12) and (13). The result is shown in Fig. 6 for salt concentration n_0 = 0.2 mol L^{-1} (a) and 0.004 mol L^{-1} (b). At the highest salt conditions (Fig. 6(a)), we immediately notice that the free energy displays

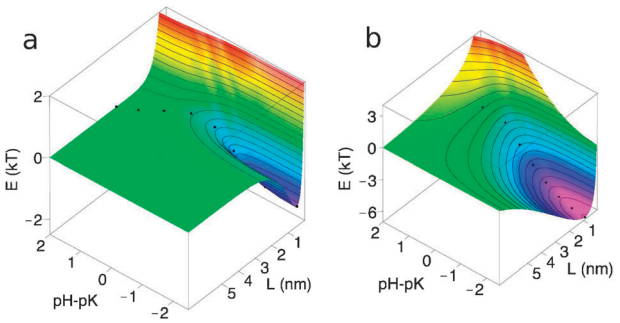

Fig. 6 Dependence of the free energy on pH–pK. Interaction free energy dependence on L and on the difference pH–pK for $\sigma^0_{\mathrm{NP}} = 0.17|\sigma_{\mathrm{DNA}}|$, for the case of bulk concentration n_{b} = 0.2 mol L^{-1} (a) and n_{b} = 0.004 mol L^{-1} (b). Energies are given in $k_{\mathrm{B}}T$ units. Dots indicate the location of minima for a few values of pH–pK.

a minimum at a NP–DNA distance close to 0.6 nm for pH lower than pK, while this minimum disappears for larger pH values. The depth of the free energy minimum is about $-5\,k_{\mathrm{B}}T$ at pH–pK = −2.5. This effect is obviously due to the fact that the effective NP charge density σ_{NP}(pH) monotonically decreases from its maximum value (low pH, *i.e.* negative pH–pK values) when pH becomes equal to pK and vanishes when pH becomes larger than pK, accordingly to eqn (11). Decreasing the salt concentration makes the free energy minimum depth larger and the free energy well wider, as shown by n_{b} = 0.004 mol L^{-1} in Fig. 6(b). The transition from the pH < pK to the pH > pK regimes results smoother.

The free energy well depth dependence on the pH conditions can be better observed by plotting the coordinates of the free energy minima, E_{min} and L_{min}, as functions of pH–pK (Fig. 7) for a large range of salt conditions, from 0.004 to 2.5 mol L^{-1}. As expected, the free energy well depth $|E_{\mathrm{min}}|$ decreases as the salt concentration increases and rapidly goes to zero for any salt when pH–pK becomes positive. Interestingly, in the pH < pK region the minimum position L_{min} is almost independent on pH–pK. It decreases with the salt concentration, but its order of magnitude does not vary significantly, being bound to the interval (0.2, 0.8). Moreover, for low salt concentrations $n_{\mathrm{b}} \leq$ 0.015 mol L^{-1}, the values of L_{min} are practically indistinguishable at our level of precision (Fig. 7, inset).

A rough analytical estimate can be given for both the well depth and position in the case of high salt concentrations. In this limit, the Debye length is such that even near the NP the counter-ion concentration is most likely the same as in the bulk, so that $\beta e\phi$ is close to zero. In this case, replacing σ_{NP} by $\sigma^0_{\mathrm{NP}}/(1 + 10^{(\mathrm{pH}-\mathrm{p}K)})$ in eqn (7) and (8) allows the minima properties to be evaluated at any pH–pK value shown as solid lines in Fig. 7. This leads to a dependence on pH–pK of the form $\ln(\sigma^0_{\mathrm{NP}}/|\sigma_{\mathrm{DNA}}|) - \ln(1 + 10^{(\mathrm{pH}-\mathrm{p}K)})$ for L_{min} and proportional to $(\sigma^0_{\mathrm{NP}}/(1 + 10^{(\mathrm{pH}-\mathrm{p}K)}))^2$ for E_{min}. These expressions reproduce the observed behavior at very high salt concentrations, but rapidly deviate from it as the salt concentration decreases, especially for L_{min} at which the approximation starts to fail at n_b < 0.1 mol L^{-1} (deviations are larger than 20%). The validity of the approximated expression for E_{min} extends roughly instead at salt concentrations larger than 0.01 mol L^{-1} (within 20%, data not shown).

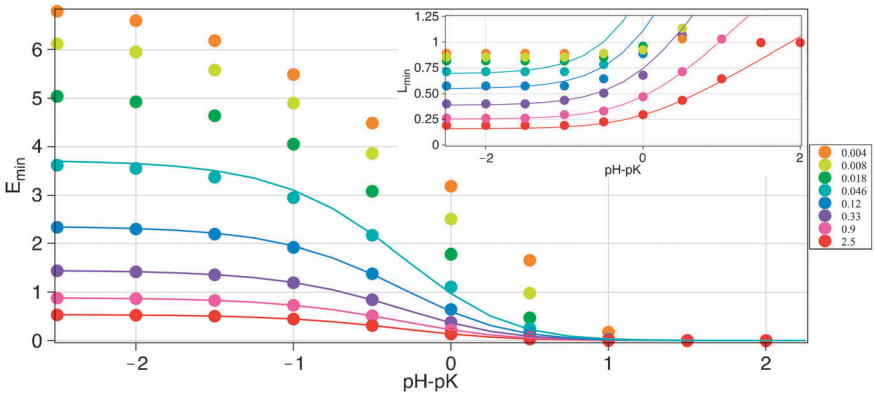

Fig. 7 Dependence on pH–pK of the position and depth of the well. The depth of the free energy well is plotted against the difference pH–pK for 15 different salt concentrations from 0.004 mol L^{-1} to 2.5 mol L^{-1} (see legend for the color code). All points are obtained by direct integration of the Poisson–Boltzmann equation with boundary conditions eqn (12) and (13) and determining numerically the minima. The NP charge density is $\sigma^0_{NP} = 0.17|\sigma_{DNA}|$. **Inset:** the position L_{min} of the minimum computed in the same conditions. Data for concentrations 0.004 to 0.012 mol L^{-1} are superposed (the resolution in the determination of L_{min} is limited by the PB integration step, *i.e.* 0.035 nm). In both graphs, the solid lines are the high salt approximations obtained by replacing σ_{NP} by $\sigma^0_{NP}/(1 + 10^{pH-pK})$ in eqn (7) and (8). Only the curves obtained for salt concentrations larger than 0.05 mol L^{-1} are plotted.

3. Local pH effect. Close to the DNA molecule, the ion concentrations are strongly modified. The H^+ concentration is also affected by the DNA charge, so that a modified *local* pH value should exist. Further modifications of the local pH are then induced by the approaching NP, due to its positive charge. In turn, the NP charge depends on the *local* pH, which is higher close to the DNA surface. Therefore, one can reasonably expect that the NP charge will increase when the NP approaches DNA.

It is interesting to investigate the effects of local pH by analyzing the concentration of hydrogen ions at the NP surface, as a function of pH–pK and of the NP distance L from the DNA surface. In order to compare to the bulk pH, we plot the quantity $-\log(n_{H+}(L))/pH$ where $n_{H+}(L)$ is the local H^+ concentration near the NP. The cases of ionic strengths 0.004 mol L^{-1} and 0.2 mol L^{-1} for NP charge density $\sigma^0_{NP} = 0.17|\sigma_{DNA}|$ are shown in Fig. 8a. For large L, the local H^+ concentration is lowered by the presence of the NP positive charge, *i.e.* the pH is locally increased at the NP surface. The increment is of course dependent on the bulk pH–pK, because the NP charge depends on this parameter. Higher salt concentrations smooth out this variability, as intuitively expected.

Interestingly, very similar behavior is observed for different NP charge densities in the range $[0.05|\sigma_{DNA}|, 0.4|\sigma_{DNA}|]$ (data not shown). When NP approaches the negative DNA surface, $n_{H+}(L)$ grows and the local pH decreases. The value close to contact (the lowest distance considered in Fig. 8 is $L = 0.05$ nm) this result is closer to the bulk pH, for low salt concentrations. In turn, local variations of pH should affect the NP charge (using eqn (11)) when approaching DNA. Since the pH decreases, we expected NP to become more charged near the DNA, and this was indeed observed solving the Poisson–Boltzmann equation with charge regulation, as shown in Fig. 8b for the same parameter choice. Again, the behavior is quantitatively very close for different values of σ^0_{NP} and n_b within the considered ranges. The most remarkable difference is that the higher the salt concentration is, the steeper the charge density rise for $L \to 0$.

In summary, local variations in the H^+ concentration induced by both the NP and DNA charges are such that,

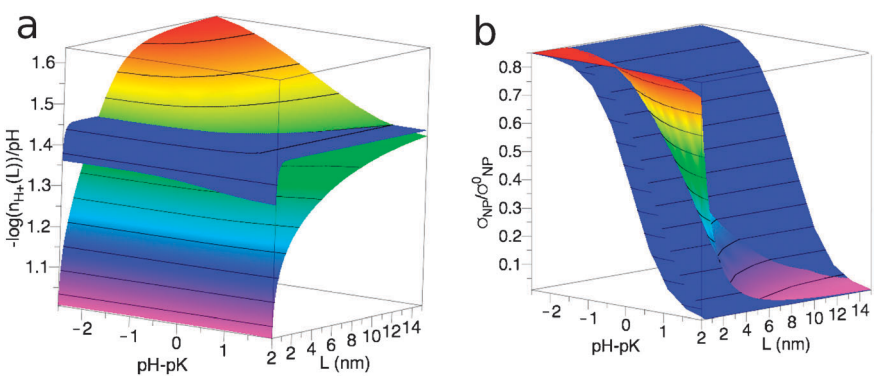

Fig. 8 Local effects at the NP surface. (a) The ratio $-\log(n_{H+}(L))/pH$ of the local over bulk pH at the NP surface, and (b) the ratio $\sigma_{NP}/\sigma^0_{NP}$ of the charge density on the NP surface over the maximum charge density, both plotted as functions of the distance L from DNA for different values of the bulk parameter pH–pK. Here $\sigma^0_{NP} = 0.17|\sigma_{DNA}|$ and the salt concentrations are $n_0 = 0.004$ M (blue surfaces) and $n_0 = 0.2$ M (multi-coloured surfaces). All data are obtained by direct integration of the modified Poisson–Boltzmann equation.

when approaching DNA, the pH-dependent NP charge density tends to recover its maximum value σ^0_{NP}. Consequently, the NP–DNA interaction becomes close, at this limit, to that observed for fixed charge NPs as described in previous sections. The short range behavior previously observed, and in particular, the presence of ion-mediated repulsion, is therefore a robust feature.

We end this section by noting that the local pH in the vicinity of DNA can be strongly affected by the presence of divalent ions. Indeed, the addition of divalent salt considerably alters the condensed counter-ion shell because divalent ions strongly compete with monovalent ones, this leads to a rapid increase of the local pH (decrease of the local H^+ concentration). Strong modulation effects should therefore be observed in divalent salts in addition to the well known fluctuation and entropic effects, and will be investigated in future work.

V. Van der Waals interactions

So far we have studied electrostatic interaction but electrodynamic interactions such as Van der Waals (VdW) forces are also known to play a role in usual colloid physics. In DLVO theory for instance, electrostatic and VdW interactions are about the same range of magnitude so that a wide class of behaviors can arise depending on the type of materials and the salt concentration.[21] It is otherwise commonly assumed that when treating the problem of NPs, such as proteins interacting with DNA or with each other, VdW interactions can be considered as negligible. However a recent work[44] has shown that the repulsive effect predicted above was not observable between mica plates of opposite charge owing to VdW interactions. This section is thus dedicated to estimating the magnitude of the VdW interactions for NP–DNA interacting systems to clarify this discrepancy.

1. Evaluation of the VdW contribution to the interaction. We consider a spherical NP of radius R_{NP}. DNA is still modeled as an infinite rigid cylinder of radius R_{DNA}. Neglecting retardation effects and assuming that each material is not too dense, the electrodynamic free energy in this non trivial geometry can be given within the pairwise additivity approximation by:[45]

$$U^{VDW}_{DNA/W/NP}(z) = -\frac{\pi A_{DNA/W/NP}}{8}\{\} \qquad (14)$$

$$\begin{aligned}\{\} = &\frac{R_{NP}^2-(z+R_{DNA})^2}{2(z+R_{DNA}+R_{NP})^2}-\frac{R_{NP}^2-(z-R_{DNA})^2}{2(z-R_{DNA}+R_{NP})^2}\\ &+\frac{R_{NP}^2-(z-R_{DNA})^2}{2(z-R_{DNA}-R_{NP})^2}-\frac{R_{NP}^2-(z+R_{DNA})^2}{2(z+R_{DNA}-R_{NP})^2}\\ &+\frac{2z+2R_{DNA}}{z+R_{DNA}+R_{NP}}-\frac{2z+2R_{DNA}}{z+R_{DNA}-R_{NP}}\\ &+\frac{2R_{DNA}-2z}{z-R_{DNA}+R_{NP}}+\frac{2z+2R_{DNA}}{z+R_{DNA}-R_{NP}}\\ &+\ln\left(\frac{z+R_{DNA}+R_{NP}}{z+R_{DNA}-R_{NP}}\right)+\ln\left(\frac{z-R_{DNA}-R_{NP}}{z-R_{DNA}+R_{NP}}\right)\end{aligned}$$

where $A_{DNA/W/NP}$ is the Hamaker constant for the DNA and the NP in the presence of water, and z is the distance between the center of the sphere and the axis of the cylinder.

The pairwise additivity approximation is valid for dilute media such as gases and is not supposed to hold for dense media interacting with each other. Rigorous derivations for various geometries have been recently proposed[46] for Casimir interactions and can in principle be extended to VdW interactions. However, they usually do not lead to explicit formulae except in limited cases where the surface-to-surface distance is either short or long with respect to the size of the particles. The advantage of the pairwise additivity approximation is thus to provide a general analytical formulae for the interaction. Actually, the distance dependence of the interaction calculated with both methods is about the same in these limiting regimes. In fact, most of the discrepancies (that can attain several orders of magnitude) between the rigorous calculation and pairwise additivity approximation reside essentially in the value of the Hamaker constant.[47] A good compromise is therefore to use a rigorous calculation for the Hamaker constant while taking into account geometrical effect through the pairwise additivity approximation.

2. Hamaker constant values for different media. When retardation effects can be neglected, *e.g.* when the surface-to-surface distance is about few nanometres, the Hamaker constant in k_BT units reads:[47]

$$A_{DNA/W/NP} = \frac{3}{2}{\sum_{n=0}^{\infty}}' \sum_{q=1}^{\infty} \frac{(\Delta^n_{DNA/W}\Delta^n_{NP/W})^q}{q^3} \qquad (15)$$

$$\Delta^n_{ab} = \frac{\varepsilon_a(i\xi_n)-\varepsilon_b(i\xi_n)}{\varepsilon_a(i\xi_n)+\varepsilon_b(i\xi_n)} \qquad (16)$$

$$\xi_n = 2\pi\frac{k_BT}{\hbar}n \qquad (17)$$

In eqn (15), $(\sum')$ means that the $n = 0$ term is multiplied by one half and the formula is valid if we consider only non magnetic materials. The sum over n is actually a sum over all the—temperature dependent—Matsubara frequencies ξ_n, as given in eqn (17), that can arise in the material. In eqn (16) $\varepsilon_a(i\xi)$ is the value of the dielectric function of the medium a when evaluated at the imaginary frequency $i\xi$. A simple phenomenological model is currently used to infer $\varepsilon(i\xi)$ that is:

$$\varepsilon(i\xi) = 1 + \sum_j \frac{d_j}{1+\xi\tau_j} + \sum_j \frac{f_j}{\omega_j^2+g_j\xi+\xi^2} \qquad (18)$$

where d_j, τ_j, f_j, g_j and ω_j are material dependent parameters that are optimized to fit experimental data for each material. Tables of these parameters for most common metallic and dielectric materials are available in ref. 47. Unfortunately, as far as we know, such a table does not exist for DNA at the frequency domain of interest and we are not aware of a simple model to predict analytically its dielectric properties. We can still guess the magnitude of interaction of the VdW interaction of DNA with a given NP assuming that DNA has dielectric properties close to the proteins. We use a table taken from ref. 48 to compute an estimate of the Hamaker constant.

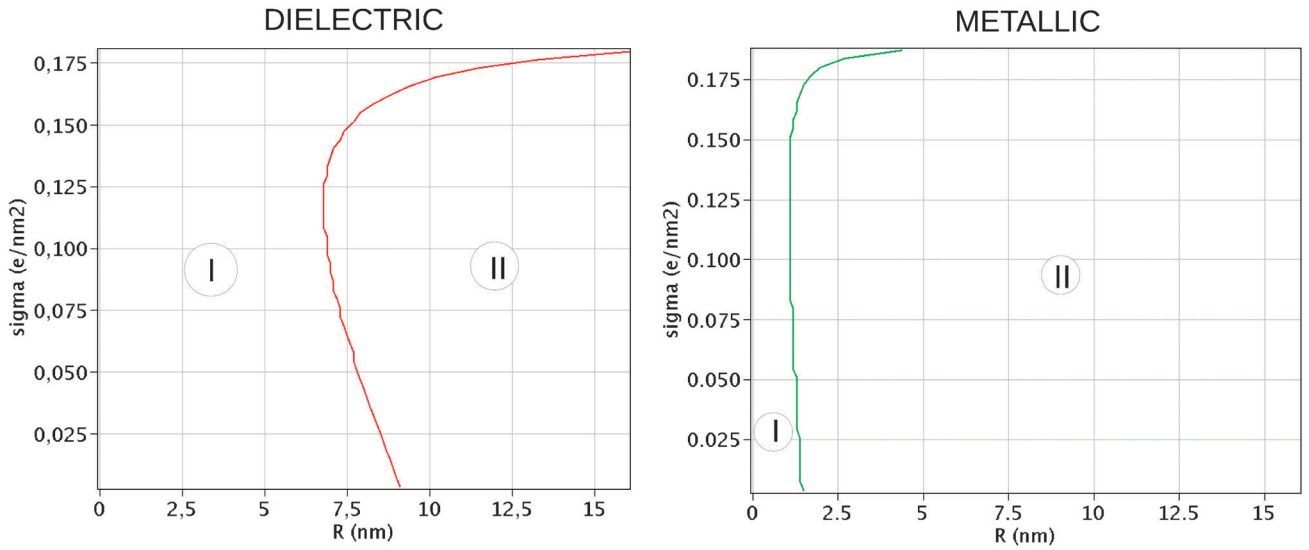

Fig. 9 Predominance diagram of VdW/Coulombic contributions. Plot of stability lines delimiting regions where the electrostatic short distance repulsion exists or disappears when taking into account VdW interactions. The red line corresponds to dielectric NPs and the green line to metallic ones. Regions denoted by the number *I* corresponds to regions where the interaction is still repulsive at short range in spite of the VdW attraction. Regions denoted by the number *II* corresponds to the opposite case where the repulsive disappears due to VdW attraction.

For gold interacting with DNA through water we find $A_{\mathrm{DNA}/W/\mathrm{GOLD}} \approx 8k_{\mathrm{B}}T$ while for protein–DNA interacting through water we find $A_{\mathrm{DNA}/W/\mathrm{PROT}} \approx 3\,k_{\mathrm{B}}T$. For silver NPs interacting with DNA through water, the result is almost the same as for gold. The Hamaker constants of dielectric materials are therefore roughly one order of magnitude less than those of metallic materials. In the following, we therefore focus on two extreme classes of materials: dielectric ones and metallic ones whose Hamaker constants are 1 $k_{\mathrm{B}}T$ and 10 $k_{\mathrm{B}}T$, respectively. It has to be mentioned that the medium between these macromolecules is not really pure water but rather an electrolyte solution. In this case low frequency terms in eqn (15) are overestimated and may be screened out by free charges in solution, decreasing the VdW interaction magnitude at the same time.

3. Magnitude of VdW interactions with respect to Coulombic ones for the systems studied here. The objective here is to determine for which kind of NP the VdW interaction brings or does not bring qualitative changes to those previously predicted. That is, characterizing each NP by its surface charge density, its radius and its dielectric function for imaginary frequencies, we look for a diagram in which one can determine whether or not VdW forces are relevant to the system. For spherical and positively charged particles, the electrostatic interaction is attractive, so that VdW interactions enhance this behavior. However, for NPs whose interface is concave and matches the DNA cylinder, it may be interesting to know whether the predicted repulsion still holds or else vanishes because of VdW forces. Moreover, since we are dealing with very short distances (~Å) the description of the system in terms of perfectly separated media is no longer valid. This has already been pointed out in the literature[47] and the abrupt separation is thought to be responsible for the well known divergence of the VdW interaction at close contact. To prevent it, a continuous description of the whole system has been proposed,[49] which shows that electrodynamic interactions do not diverge and anymore at close contact. In our situation, water is structured around each macromolecule, so that its dielectric properties are not the same in these regions. It somehow allows the dielectric function of the system to vary continuously from one medium to another. The typical width of this structured water is about two molecule layers *i.e.* ~5 Å. In the following, we therefore assume that for distances above ~5 Å, eqn (14) holds and that below this characteristic length the magnitude of the interaction saturates until close contact.[50] In Fig. 9, we vary the surface charge density and the size of the NP for each class of material to determine whether the VdW attraction kills or else preserves the short range repulsion. In conclusion, the repulsive effect is very robust for dielectric NPs for a wide range of sizes, whereas for metallic NPs, it only exists for very small sizes, *i.e.* below ~2 nm. This actually agrees well with previous observations on protein chromatography.[51]

Conclusions

In this study, initially motivated by the observation that the shape of DNA-binding proteins is often highly complementary with DNA, we have dissected the physical interaction between NP and DNA into its most relevant contributions. At the nanoscale of NP, VdW attraction has been shown to be weak enough to preserve the short range repulsion recently evidenced between DNA and proteins, and is summarized in the predominance diagram in Fig. 9.

This short range repulsion is specific to indented particles and is a robust property that holds for a large range of materials and charge densities; dielectric materials being more prone to this repulsion than metals. Charge regulation for pH-dependent charge surface density has been considered in

detail and shown to preserve also the essential features of fixed charge NP. The major determinant of the interaction between NP and DNA is definitely NP shape.

Positively charged NP with convex shapes and high enough charge surface densities may stick onto DNA irreversibly, or at least with a higher affinity than any protein, either transcription factors or histone-like proteins. This will result in genotoxic effects due to competitive inhibition. Indeed, such NPs are used as bactericides[16,17] but are generally harmless to humans (and to eukaryotes in general) because they are stopped by proteins[52] and stored into the lysosomes instead of entering the nucleus. However, in some cases this protection mechanism breaks down or is simply overtaken, and genotoxic effects are likely to occur. Conversely an indented (concave) NP should not be as harmful because they are prone to short range repulsion. Finally a convex or concave NP may be also conveyed by "trojan NP" into the nucleus for a therapeutic purpose.[15]

The theory proposed in this paper gives a rationale basis for discussing the interaction of NP with DNA and attempts to provide a guide to tailoring NP from observations made on proteins

References

1 R. B. Winter, O. G. Berg and P. H. von Hippel, *Biochemistry*, 1981, **20**, 6961.
2 M. Coppey, O. Bénichou, R. Voituriez and M. Moreau, *Biophys. J.*, 2004, **87**, 1640.
3 N. Shimamoto, *J. Biol. Chem.*, 1999, **274**, 15293.
4 I. Bonnet, A. Biebricher, P.-L. Porté, C. Loverdo, O. Bénichou, R. Voituriez, C. Escudio, W. Wende, A. Pingoud and P. Desbiolles, *Nucleic Acids Res.*, 2008, **36**, 4118.
5 C. Loverdo, O. Benichou, R. Voituriez, A. Biebricher, I. Bonnet and P. Desbiolles, *Phys. Rev. Lett.*, 2009, **102**, 188101.
6 S. Jones, P. van Heyningen, H. M. Berman and J. M. Thornton, *J. Mol. Biol.*, 1999, **287**, 877.
7 K. Nadassy, S. J. Wodak and J. Janin, *Biochemistry*, 1999, **38**, 1999.
8 Y. Takeda, P. D. Ross and C. P. Mudd, *Proc. Natl. Acad. Sci. U. S. A.*, 1992, **89**, 8180.
9 P. H. Von Hippel, *Annu. Rev. Biophys. Biomol. Struct.*, 2007, **36**, 79.
10 H. Viadiu and A. Aggarwal, *Mol. Cell*, 2000, **5**, 889.
11 C. G. Kalodimos, N. Biris, A. M. J. J. Bonvin, M. M. Levandoski, M. Guennuegues, R. Boelens and R. Kaptein, *Science*, 2004, **305**, 386.
12 V. Dahirel, F. Paillusson, M. Jardat, M. Barbi and J.-M. Victor, *Phys. Rev. Lett.*, 2009, **102**, 228101.
13 F. Bertorelle, C. Wilhelm, J. Roger, F. Gazeau, C. Menager and V. Cabuil, *Langmuir*, 2006, **22**, 5385.
14 M.-S. Martina, J.-P. Fortin, L. Fournier, C. Menager, F. Gazeau, O. Clement and S. Lesieur, *Mol. Imaging*, 2007, **6**, 140.
15 N. Tsapis, D. Bennett, B. Jackson, D. A. Weitz and D. A. Edwards, *Proc. Natl. Acad. Sci. U. S. A.*, 2002, **99**, 12001.
16 V. Thomas, Murali Mohan Yallapu, B. Sreedhar and S. K. Bajpai, *J. Colloid Interface Sci.*, 2007, **315**, 389.
17 J. R. Morones, J. L. Elechiguerra, A. Camacho, K. Holt, J. B. Kouri, J. T. Tapia Ramirez and M. J. Yacaman, *Nanotechnology*, 2005, **16**, 2346.
18 A.-M. Florescu and M. Joyeux, *J. Chem. Phys.*, 2009, **130**, 015103.
19 O. Givaty and Y. Levy, *J. Mol. Biol.*, 2009, **385**, 1087.
20 A. G. Cherstvy, A. B. Kolomeisky and A. A. Kornyshev, *J. Phys. Chem. B*, 2008, **112**, 4741.
21 J. Vervey and J. T. G. Overbeek, *Theory of the Stability of Lyophobic Colloïds*, Elsevier, Amsterdam, 1948.
22 S. Safran, *Statistical Thermodynamics of Surfaces, Interfaces, and Membranes*, Westview Press, 2003.
23 J.-P. Hansen and H. Lowen, *Annu. Rev. Phys. Chem.*, 2000, **51**, 209.
24 C. Myung-Suk and W. R. Bowen, *J. Colloid Interface Sci.*, 2004, **272**, 330.
25 P.-G. de Gennes, *ScalingConcept in Polymer Physics*, Cornel Univeristy Press, 1979.
26 S. Jones, H. P. Shanahan, H. M. Berman and J. M. Thornton, *Nucleic Acids Res.*, 2003, **31**, 7189.
27 E. Allahyarov, I. D'Amico and H. Löwen, *Phys. Rev. Lett.*, 1998, **81**, 1334.
28 J. Z. Wu, D. Bratko and J. M. Prausnitz, *Proc. Natl. Acad. Sci. U. S. A.*, 1998, **95**, 15169.
29 A. Naji, S. Jungblut, A. G. Moreira and R. R. Netz, *Phys. A*, 2005, **352**, 131.
30 V. Dahirel, M. Jardat, J.-F. Dufrêche and P. Turq, *Phys. Chem. Chem. Phys.*, 2008, **10**, 5147.
31 M. Lund, B. Jönsson and C. E. Woodward, *J. Chem. Phys.*, 2007, **126**, 225103.
32 M. E. Davis and A. McCammon, *J. Comput. Chem.*, 1991, **12**, 909.
33 S. Tyagi, M. Süzen, M. Sega, M. Barbosa, S. S. Kantorovich and C. Holm, *J. Chem. Phys.*, 2010, **132**, 154112.
34 V. Dahirel, M. Jardat, J.-F. Dufrêche and P. Turq, *Phys. Rev. E: Stat., Nonlinear, Soft Matter Phys.*, 2007, **76**, 040902.
35 V. Dahirel, M. Jardat, J.-F. Dufrêche and P. Turq, *J. Chem. Phys.*, 2007, **127**, 095101.
36 M. N. Tamashiro and H. Schiessel, *Phys. Rev. E: Stat., Nonlinear, Soft Matter Phys.*, 2003, **68**, 066106.
37 A. Abrashkin, D. Andelman and H. Orland, *Phys. Rev. Lett.*, 2007, **99**, 077801.
38 F. Paillusson, M. Barbi and J.-M. Victor, *Mol. Phys.*, 2009, **107**, 1379.
39 M. Kanduc, M. Trulsson, A. Naji, Y. Burak, J. Forsman and R. Podgornik, *Phys. Rev. E: Stat., Nonlinear, Soft Matter Phys.*, 2008, **78**, 061105.
40 A. G. Moreira and R. R. Netz, *Europhys. Lett.*, 2000, **52**, 705.
41 G. Tellez and E. Trizac, *J. Stat. Mech.*, 2006, **6**, 06018.
42 D. Ben-Yaakov, Y. Burak, D. Andelman and S. A. Safran, *Europhys. Lett.*, 2007, **79**, 48002.
43 B. W. Ninham and V. A. Parsegian, *J. Theor. Biol.*, 1971, **31**, 405.
44 N. Kampf, D. Ben-Yaakov, A. Andelman, S.-A. Safran and J. Klein, *Phys. Rev. Lett.*, 2009, **103**, 118304.
45 S. W. Montgormey, M. A. Franchek and V. W. Goldschmidt, *J. Colloid Interface Sci.*, 2000, **227**, 567–587.
46 S. J. Rahi, T. Emig, N. Graham, R. L. Jaffe and M. Kardar, *Phys. Rev. D*, 2009, **80**, 085021.
47 V. A. Parsegian, *Van der Waals Forces*, Cambridge University Press, 2006.
48 C. M. Roth, B. L. Neal and A. M. Lenhoff, *Biophys. J.*, 1996, **70**, 977.
49 R. Podgornik and V. A. Parsegian, *J. Chem. Phys.*, 2004, **121**, 7467.
50 J. Stahlberg, B. Jonsson and C. Horvath, *Anal. Chem.*, 1992, **64**, 3118.
51 B. Jonsson and J. Stahlberg, *Colloids Surf., B*, 1999, **14**, 67.
52 I. Sondi and B. Salopek-Sondi, *J. Colloid Interface Sci.*, 2004, **275**, 177.